Geol. Mag. **144** (*1*), *2007, pp. 53–65. © 2006 Cambridge University Press*
doi:10.1017/S001675680600269X First published online 19 October 2006 *Printed in the United Kingdom*

Amethyst-bearing lava flows in the Paraná Basin (Rio Grande do Sul, Brazil): cooling, vesiculation and formation of the geodic cavities

DOMINIQUE PROUST* & CLAUDE FONTAINE

UMR 6532 CNRS, HydrASA, Faculté des Sciences, 40 Avenue du recteur Pineau, 86022 Poitiers cedex, France

(*Received* 6 January 2006; *accepted* 13 March 2006)

Abstract – Size distribution data obtained from detailed field study of bubbles and amethyst-geodes in the basaltic lava flows of the Serra Geral Formation (Ametista do Sul, Rio Grande do Sul, Brazil) are used in cooling and vesiculation models to infer the origin and the formation processes of the geodic cavities. Coupled field observations and modelling results emphasize that (1) the formation of geodes in the studied lava flow can be explained, qualitatively and quantitatively, by the exsolution of magmatic gas from the supersaturated melt with no need for external surface water supply; (2) the vertically elongated habits of the geodes result from higher cooling rate of the magma in contact with the accumulating bubbles; and (3) the abnormal metre-sized geodes with their branching habits result not only from the diffusive/decompressive bubble growth but also from the coalescence of inwards-progressing tubular cavities.

Keywords: lava flows, basalts, volcanic rocks, mineralogy, amethyst, geodes, vesiculation.

1. Introduction

The successive lava flows which poured out during the continental flood volcanism in the Paraná basin built up the volcanic pile of the Serra Geral Formation covering about 1 200 000 km^2 (Fig. 1a). The volcanic pile has a present total thickness ranging from 350 m at the basin borders up to 1723 m in its central part. The ^{40}Ar–^{39}Ar study of the basaltic rocks gives lower Cretaceous dates, from 137 Ma to 127 Ma (Turner *et al.* 1994). These data, together with the palaeomagnetic results (Bellieni *et al.* 1984; Ernesto & Pacca, 1988), suggest that the Paraná flood volcanism was related to the geodynamic process which led to the South America–Africa breakup (opening of the southern Atlantic Ocean) and the production of a typical oceanic crust. The volcanic pile of the Serra Geral Formation actually appears as a succession of stacked cooling units intercalated with continental aeolian sandstones. These sandstones result from the erosion of the Botucatú Formation formed at the end of the sedimentation process in the Paraná basin (Triassic–Jurassic). The thickness of the lava flows ranges from a few metres to one hundred metres (Melfi, Piccirillo & Nardy, 1988). The volcanic products are represented by (1) basic rocks with tholeiitic basalts and tholeiitic basaltic andesites (70 vol. %); (2) intermediate rocks with tholeiitic andesites, lati-andesites and latites (7 vol. %); and (3) overlying acidic rocks with rhyodacites and rhyolites (3 vol. %). The thick tholeiitic basaltic flows in South Brazil and Uruguay are famous for their large-sized amethyst crystals which are found as partial fillings of geodic cavities included in the massive upper part of the flows. Although magma degassing and vesiculation are well-known physical processes, the origin of these unusually large geodic cavities (up to 2.50 m in height with a peculiar cone-shaped habit) is still debated. The two main proposals are: (1) epigenetic geode formation at temperature below 150 °C due to an explosive event with hydraulic basalt fracturing by fluids originated from the Guarany sediments aquifer (Duarte, Hartmann & Vasconcellos, 2005), (2) magmatic gas exsolving from the supersaturated melt with respect to dissolved volatiles (Scopel *et al.* 1998; Gilg *et al.* 2003). The present study was initiated in order to discuss the formation processes of the geodic cavities with the debated question about the origin of water vapour. The study coupled the modelling of magma cooling and vesiculation and field observations, that is, the size and the distribution of the vesicles and geodes within a thick amethyst-bearing lava flow.

* Author for correspondence: dominique.proust@hydrasa.univ-poitiers.fr

2. Basaltic flow

The amethyst-bearing lava flows found in the southern Paraná basin belong to the volcanic Serra Geral Formation, made up of tholeiitic basalts. The studied area is located near Ametista do Sul (Rio Grande do Sul), the principal place mined for amethyst. A sequence of five flat-lying basic lava flows, 10 to 50 m thick, is exposed along a steep road-cut, 1 km east of Ametista do Sul. The amethyst geodes are found in the upper part of the two thickest

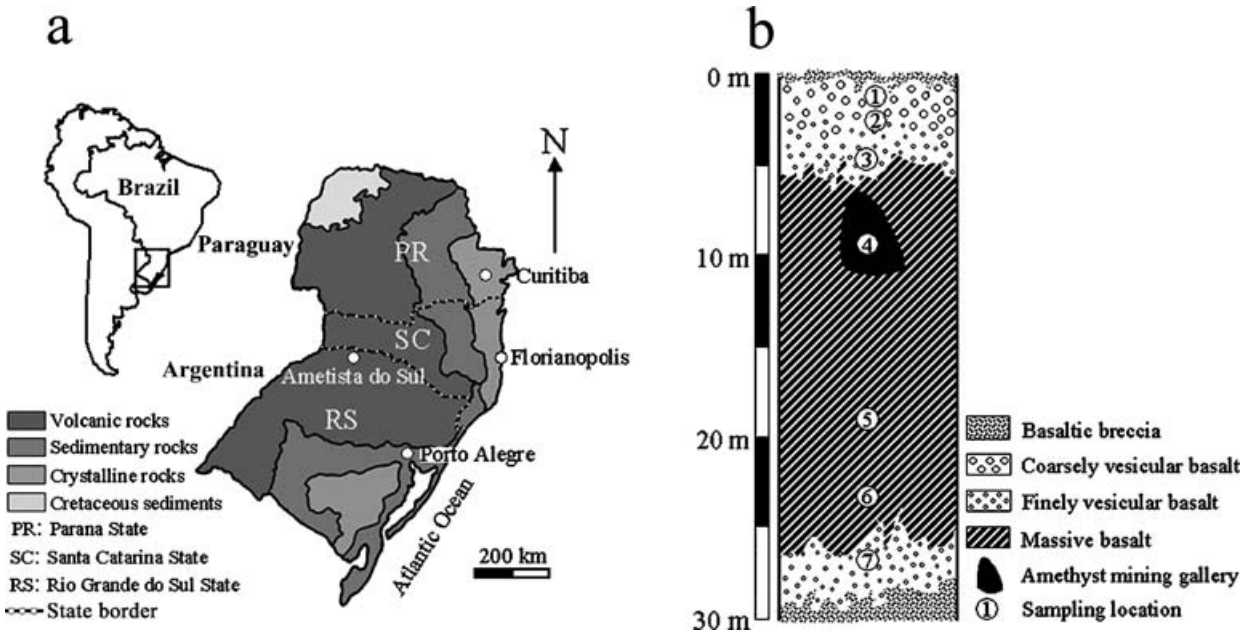

Figure 1. Geological setting and geode-bearing lava flow: (a) geographical and geological settings of the Paraná basin; (b) vertical cross-section of the geode-bearing lava flow in Triz quarry.

flows (30 m and 50 m). The studied flow is 30 m thick and exposed on the Triz quarry working-face (27°21′38.42″ S, 53°09′37.84″ W), east of Ametista do Sul (Fig. 1a, b). The amethyst geodes are located in the upper 10 m, at the top of the hosting massive tholeiitic basalt. The Triz lava flow is intercalated between two reddish, 1 m thick, aeolian sandstone levels which grade inwards to basaltic breccia. No prismatic jointing occurs at the outcrop, but a massive, vesicle-free central part, about 20 m thick (samples 4, 5 and 6 in Fig. 1b), is intercalated between two greenish-brown vesicular levels. These two vesicular levels are organized differently at the outcrop: the upper level is thicker (5 m), grading from a finely vesicular basalt in contact with the inner massive central part (sample 3) to a coarsely vesicular basalt at the top of the flow (samples 1 and 2); the lower vesicular level is thinner (2 m) and entirely made up of a finely vesicular basalt (sample 7). The amethyst level is at the top of the massive central part, with 3 m maximum thickness, its lower part being at 10 m depth in the lava flow. The geodic cavities display a dominant vertical tubular habit with downwards-increasing diameter, with a 0.3 m average height, although metre-sized geodes could be found locally.

3. Analytical methods

3.a. Modelling the thermal history of the lava flow

Most of what is known about the thermal regime in a cooling magma has been obtained from numerical conductive or convective heat-transfer models (Jaeger, 1961, 1968; Hardee & Dunn, 1981; Long & Wood, 1986; Reiter *et al.* 1987; Degraff, Long & Aydin, 1989; Philpotts & Dickson, 2002; Patrick, Dehn & Dean, 2004). These models were tested in active natural systems like the lava lakes of Kilauea Volcano to validate the modelling of lava cooling and fracturing (Peck, Hamilton & Shaw, 1977; Peck, 1978) as well as degassing and vesiculation (Gerlach, 1986; Mangan, Cashman & Newman, 1993; Cashman, Mangan & Newman, 1994). Numerous studies demonstrated that most of the structures and textures observed in ancient solidified lava flows resulted from these cooling processes (Long & Wood, 1986; Grossenbacher & McDuffie, 1995; Lore, Huajian-Gao & Aydin, 2000). The temperature regimes in the cooling lava flow are modelled in two stages: (1) the temperature regime during the magma solidification episode, including emission of the latent heat of crystallization over the temperature range between the liquidus (T_L) and the solidus (T_S) temperatures and (2) the temperature regime during diffusive cooling of the solidified magma, when latent heat is no longer released, down to the ambient temperature (T_A). The liquidus and solidus temperatures used herein are respectively 1200 °C and 980 °C in order to maximize solidification duration time and consequently to maximize the processes of vesicle formation and ascent in the flow. In these conditions, magma degassing is maximal and the quantity of volatiles available for geodic cavity formation is minimal. As a consequence, if this minimum volatile quantity is sufficient to simulate the geodes observed at the outcrop, then the modelling will be pertinent. The initial conditions and the values of the lava physical properties used in the calculations are summarized in Table 1.

https://doi.org/10.1017/S001675680600269X Published online by Cambridge University Press

Table 1 Initial conditions and lava properties used in the cooling model

Parameters	Symbols	Values	References
Initial conditions			
Liquidus temperature (°C)	T_L	1200	Anderson *et al.* 1984
Solidus temperature (°C)	T_S	980	Degraff, Long & Aydin, 1989
Ambient temperature (°C)	T_A	20	Peck, 1978
Lava properties			
Latent heat (J/kg)	L	3.35×105	Peck, 1978
Specific heat of liquid lava (J/(kg · °C))	c_2	1255	Jaeger, 1968
Specific heat of solidified lava (J/(kg · °C))	c_1	1050	Long & Wood, 1986
Thermal conductivity (J/(m · s · °C))	K	1.10	Long & Wood, 1986
Density of liquid lava (kg/m^3)	ρ_2	2600	Jaeger, 1968
Density of solidified lava (kg/m^3)	ρ_1	2830	Murase & McBirney, 1973
Basalt properties			
Equivalent molar mass (g)	M_e	363.51	This study
Equivalent molar volume (cm^3)	V_e	139.81	This study

3.b. Modelling the vesiculation of the lava flow

The vesicle population observed in solidified subaerial lava flows is the integrated result of several physical processes which have been intensively studied and modelled (Sparks, 1978; Sahagian, 1985; Aubele, Crumpler & Elston, 1988; McMillan, Long & Cross, 1989; Sahagian, Anderson & Ward, 1989; Toramaru, 1989; Walker, 1989; Bottinga & Javoy, 1990; Goff, 1996; Beresford *et al.* 2000): (1) the degassing, mainly by depressurization, of the ascending magma which induces the bubble nucleation by exsolution of the volatile components initially dissolved in the magma at depth, (2) the bubble growth by diffusion of volatile components and by expansion due to depressurization, (3) the bubble ascent which is controlled by the bubble size and the increasing viscosity of the cooling magma, and (4) the bubble coalescence. The result of the degassing model is to estimate the global amount of water vapour, both the vapour at once dissipated in the atmosphere and that maintained in the flow for bubble formation. It gives, however, no information about the amount of water vapour involved in the bubble nucleation, growth and ascent during and after the surface degassing of the lava. Such information is obtained by bubble growth, ascent and coalescence modelling associated with geode and vesicle size distributions observed at outcrop and in rock samples (Fig. 2a, b). The diameters of the geodic cavities were measured on photographs from five mining galleries in the Triz quarry using a Macintosh-based image analysis system (Optiscan(c) and Optilab(c) software). The same procedure was used for vesicle distribution in the thin-sections of the vesicular levels (samples 1, 3 and 7 in Fig. 2b).

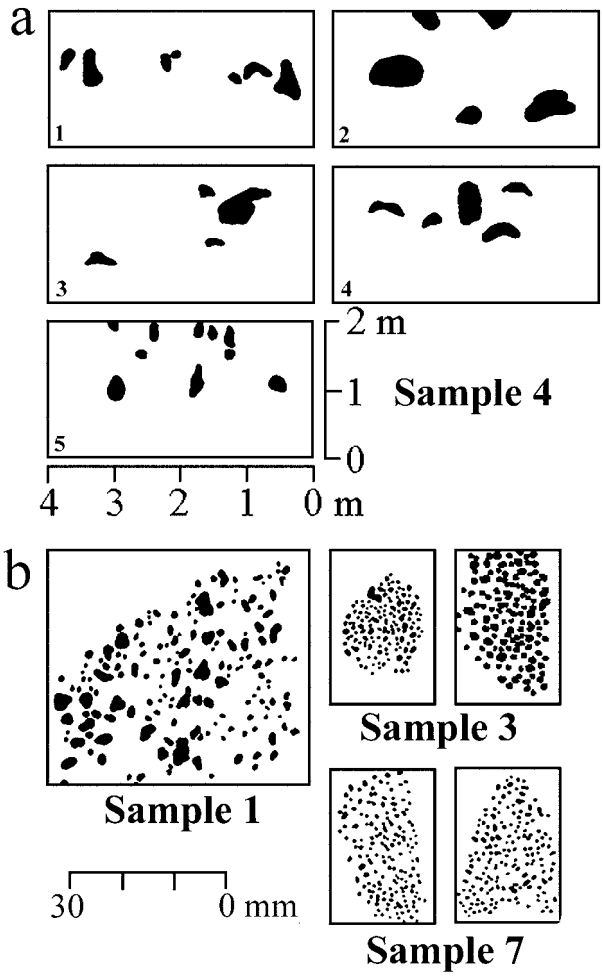

Figure 2. Geode and vesicle size distributions in the lava flow: (a) distribution of the geodic cavities (black area) along five mining galleries at the level of sample 4; (b) distribution of the vesicles (black area) on thin-sections of the vesiculated layers (samples 1, 3 and 7).

4. Solidification of the lava flow

A tabular lava flow emplaced rapidly on a rock substrate begins to cool from inwards-advancing upper and lower solidification fronts. The temperature distribution with time may be analysed by dividing the lava flow into upper and lower solidifying regions. This cooling model, however, can only be applied to ponded lava flows which are not inflated by post-emplacement lava transport through internal lava tubes between solidified upper and lower crust. Cashman & Kauahikaua (1997) have studied an inflated Pahoehoe lava flow in

https://doi.org/10.1017/S001675680600269X Published online by Cambridge University Press

Kalapana, Hawaii, and compared its internal structure and bubble distribution to ponded lava flows. The major differences between inflated and ponded lava flows lie in the upper vesicular level characteristics. The upper vesicular level in inflated flow constitutes 40 to 60 % of the total flow thickness in relation to the downward upper crust cooling and its continued uplift by lava supply in the tube. If the inflation process had operated during the Triz flow emplacement, it would have produced an upper crust with 12 to 18 m thickness instead of 5 m. Moreover, bubble distribution in the upper vesicular level of inflated lava flows shows a general decrease in vesicle number and increase in vesicle size with depth. This distribution is reversed in the Triz lava flow with increasing vesicle size and decreasing vesicularity upward. Finally, the existence of large geodic cavities in the Triz flow is in contradiction with the inflation process, where increasing lithostatic overpressure due to increasing upper crust thickness decreases volatile exsolution from the magma to form bubbles. These differences in upper level vesicularity and thickness between the Triz flow and inflated flow and the occurrence of a level with geodic cavities support the idea that the Triz flow was emplaced without active inflation processes and allows the use of the cooling model described below.

4.a. Solidification from the top of the lava flow

The position of the upper solidification front as a function of cooling time is calculated using the equation of Jaeger (1968), including emission of the latent heat of crystallization over the liquidus and the solidus temperature range,

$$x = 2\lambda_1(\mathrm{k}_1 t)^{0.5} \tag{1}$$

where x (m) is the depth of the solidified crust from the surface, λ_1 is a constant, k_1 (m^2/s) is the thermal diffusivity of the solidified lava and t (s) is the cooling time duration. Assuming that lava thermal conductivity is K = 1.10 J/(m.s. °C) (Table 1), λ_1 is calculated by solving the equation

$$(1 - \mathrm{erf}\,\mathrm{p}\,\lambda_1)\exp\left\{(\mathrm{p}^2 - 1)\lambda_1^2\right\} = \{\mathrm{pK}(T_\mathrm{L} - T_\mathrm{S})/\mathrm{K}T_\mathrm{S}\}\mathrm{erf}\,\lambda_1 \tag{2}$$

where $\mathrm{p} = (\mathrm{k}_1/\mathrm{k}'_2)^{0.5}$, $\mathrm{k}_1 = \mathrm{K}/\rho_1\mathrm{c}_1$, $\mathrm{k}'_2 = \mathrm{K}/\rho_2\mathrm{c}'_2$. The specific heat of the liquid lava including latent heat emission, c'_2, is calculated over the temperature range between liquidus and solidus from the equation given by Jaeger (1968)

$$\mathrm{c}'_2 = \mathrm{c}_2 + \mathrm{L}/(T_\mathrm{L} - T_\mathrm{S}) \tag{3}$$

where c_2 is the specific heat and L is the latent heat of the liquid lava, assumed to be uniformly liberated over the considered temperature range. Given the parameters in Table 1, and solving equation 2, $\lambda_1 = 0.72$ and equation 1 becomes

$$x = 4.92\,t^{0.5} \tag{4}$$

where x (m) is the depth of the solid crust at time t (in years) after cooling began.

4.b. Solidification from the contact with the rock substrate

The position of the lower solidification front can be calculated using

$$x = 2\,\lambda_2(\mathrm{k}_1 t)^{0.5} \tag{5}$$

with λ_2 the root of

$$(1 - \mathrm{erf}\,\mathrm{p}\lambda_2)\exp\left\{(\mathrm{p}^2 - 1)\lambda_2^2\right\} = \{\mathrm{pK}(T_\mathrm{L} - T_\mathrm{S})/\mathrm{K}T_\mathrm{S}\}(1 + \mathrm{erf}\,\lambda_2) \tag{6}$$

Using the parameters in Table 1, and solving equation 6, $\lambda_2 = 0.38$ and equation 5 becomes

$$x = 2.62\,t^{0.5} \tag{7}$$

where x (m) is the depth of the solid crust at time t (in years) after cooling began.

4.c. Solidification progress as a function of cooling time

Equations (4) and (7) are combined to simulate the progress of the upper and lower solidification fronts in the lava flow as a function of cooling time (Fig. 3a). The total solidification of the lava flow is obtained after 12 years cooling time as also observed by Scopel *et al.* (1998). Similar total solidification times are obtained using the heat diffusion models of Reiter *et al.* (1987) and Degraff, Long & Aydin (1989), that is, 10.80 and 11.20 years, respectively. The solidus isotherms (980 °C) progressing from top and bottom of the flow intersect at 18.70 m depth, approximately two-thirds of the way from the top (0.62), as previously observed by Long & Wood (1986) and McMillan, Cross & Long (1987). This indicates that the bottom of the lava flow cools more slowly than does the top, due to higher temperature at the contact between the lava flow and the rock substrate than at the free surface. The contact temperature (T_C) (in this case, contact with an earlier flow) can be calculated from the equation of Jaeger (1968):

$$T_\mathrm{C} = T_\mathrm{S}/(1 + \mathrm{erf}\,\lambda_2) = 654\,^\circ\mathrm{C} \tag{8}$$

The positions of the solidus isotherms in the studied lava flow as a function of cooling time are used to simulate the sequential development of the actually observed flow structure units (Fig. 3b). For each level, the solidification time duration and rate are, respectively: (1) 0.3 year and 0.11 cm/h for the upper coarsely vesicular level, (2) 0.4 year and 0.03 cm/h for the lower finely vesicular level, (3) 0.9 year and 0.04 cm/h for the upper finely vesicular level, (4) 1.7 years and 0.03 cm/h for the massive, vesicle-free

https://doi.org/10.1017/S001675680600269X Published online by Cambridge University Press

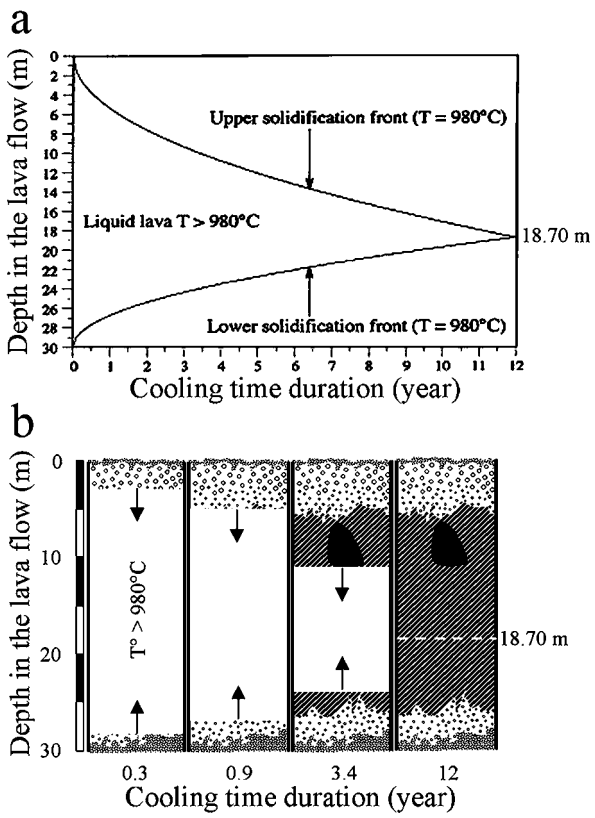

Figure 3. Solidification progress of the amethyst-bearing basaltic flow as a function of cooling time duration: (a) solidus isotherm (980 °C) position in the cooling lava is calculated by heat thermal conduction process alone; positions are computed from equations 4 and 7 (see text); parameters as given in Table 1; (b) sequential development of the flow structure units as a function of upper and lower solidification front positions with time. Symbols as in Figure 1b.

level above the amethyst geodes, (5) 3.4 years and 0.02 cm/h for the amethyst geodes level, and finally (6) 12 years and 0.01 cm/h for the massive, vesicle-free level located below the amethyst geodes. The average velocities of the upper and lower solidification fronts are 0.042 cm/h and 0.028 cm/h, respectively, in good agreement with the velocities inferred for a lava flow with thickness similar to that of the Giant's Causeway (Degraff, Long & Aydin, 1989). From these results, it can be concluded that 12 years will be the maximum time duration for vesicle nucleation, growth, coalescence and geodic cavity formation before 'bubble freezing'.

5. Vesiculation of the lava flow

5.a. Degassing of the lava flow

The major volcanic gases emitted during eruptions are H_2O, CO_2, SO_2 and H_2 with predominant H_2O and CO_2 (Sigvaldason & Elisson, 1968; Moore, 1970; Anderson, 1975; Harris & Anderson, 1983; Gerlach, 1986). The gas compositions are highly variable, mainly as a function of CO_2/H_2O ratio. Due to the lower solubility of CO_2 relative to H_2O in magmatic conditions, initial degassing at $P > 100$ bars produces CO_2-dominated bubbles (Stolper & Holloway, 1988; Bottinga & Javoy, 1990) which are rapidly exsolved during magma ascent and lost in the atmosphere at the time of subaerial flow emplacement. Later near-surface degassing (30 to 3 bars pressure) exsolves H_2O-dominated gas (80 mole % H_2O, 16 mole % S, and 4 mole % CO_2: Mangan, Cashman & Newman, 1993). Since the present paper deals with subaerial lava flow, H_2O will be the only vesicle-forming component considered in the surface degassing model.

The experimental solubility data of water in basaltic melts (Burnham & Jahns, 1962; Hamilton, Burnham & Osborn, 1964) are related to pressure (Burnham, 1979; Anderson *et al.* 1984) by

$$X_m = \exp(0.4895 \ln P - 4.25) \quad (9)$$

where X_m is the mole fraction of water dissolved in the melt and P (bar) is the confining pressure. The mass fraction C_m of water dissolved in the melt is related to its mole fraction by

$$C_m = 18.02\, X_m/(M_e - X_m(M_e - 18.02)) \quad (10)$$

where M_e is the equivalent molar mass of the anhydrous magma calculated according to Burnham (1979). The anhydrous equivalent molar mass and volume (V_e) calculated for the Triz tholeiitic basalt (Table 1) are very close to the data obtained by Burnham (1979) from the Columbia River basalt analysis of Hamilton, Burnham & Osborn (1964) and will be used as reference in the vesiculation modelling herein. The number of moles of water dissolved at a given confining pressure is then calculated per one litre of basaltic melt by

$$N_m = 1000\, X_m/\text{molar volume} \quad (11)$$

This gives $N_{m,30} = 0.29$ moles of water initially dissolved in one litre of magma at the time of its subaerial emplacement at the bottom of the flow (30 m below the top). The number of moles still dissolved in the melt at a given depth x ($N_{m,x}$) is then calculated throughout the entire lava flow with a 10 cm distance interval to account for the one litre unit volume reference (Fig. 4a). As a consequence, the number of moles exsolved as H_2O vapour with decreasing pressure at a given depth x ($N_{v,x}$) will be given by

$$N_{v,x} = N_{m,30} - N_{m,x} \quad (12)$$

The volume of H_2O vapour released at a given depth in the flow is calculated using the ideal gas law $P\,V = N_{v,x}\,RT$ where P is the confining pressure (atm), $N_{v,x}$ the number of H_2O exsolved moles at a depth x, R the gas constant (0.082 atm dm^3/(K · mole), and T the temperature in K (Fig. 4b). The net result of this degassing model is to estimate the global amount of water vapour, including that dissipated in the atmosphere and that maintained in the flow for bubble

https://doi.org/10.1017/S001675680600269X Published online by Cambridge University Press

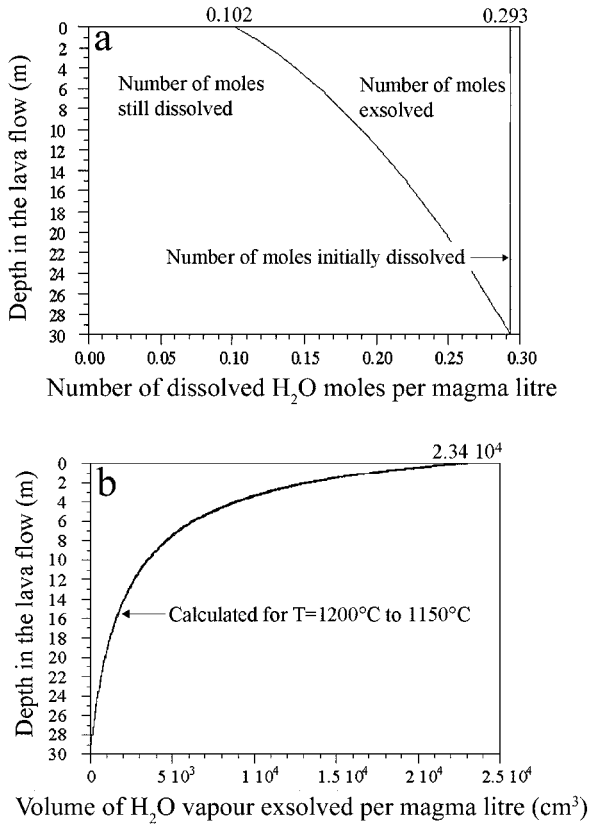

Figure 4. Amount of water (dissolved in the magma or exsolved as vapour) available in the lava flow at time of its emplacement: (a) number of moles of water dissolved or exsolved as vapour as a function of depth in the flow; (b) volume of water vapour exsolved as a function of depth in the flow; superimposed curves were calculated for $T = 1200$ to 1150 °C with 10 °C temperature interval.

formation. It gives no precise information, however, about the amount of water vapour actually involved in the bubble nucleation, growth and ascent during and after the surface-degassing of the lava. Such data can be obtained from the vesicle size distribution and the bubble ascent modelling.

5.b. Vesicle size distribution

The vesicle diameters were measured on photographs from vesicular-level thin-sections. The two-dimensional data were converted to three-dimensional values using the methods of Cashman & Marsh (1988). The size frequency diagrams (open circles, Fig. 5a, b, c) characterize unimodal vesicle populations changing from well-sorted, almost Gaussian distribution, at the bottom of the flow (Fig. 5c) to distributions which are progressively stretched toward larger size fractions in the upper levels, with a maximum stretch at the top (Fig. 5a). The mean and maximum bubble diameters increase from the bottom (0.14–0.27 cm) to the top of the flow (0.23–0.81 cm). These vesicle size distributions match the morphological observations at the outcrop and are currently observed in subaerial lava flows (e.g. Sahagian, 1985; Sahagian, Anderson & Ward, 1989; Walker, 1989). The cumulative vesicle number diagrams (solid circles, Fig. 5a, b, c) display two distinct patterns on both sides of the median diameter which remains unchanged throughout the lava flow (0.12 to 0.14 cm): (1) bubbles with diameters smaller than the median diameter have similar cumulative curves with nearly constant slopes and modal diameter close to the median diameter, that is, the same size distribution occurs in the entire lava flow, but with decreasing bubble frequency; (2) bubbles with diameters larger than the median diameter have cumulative curves progressively stretched toward larger sizes with decreasing slopes from the bottom to the top of the flow. These patterns are indicative of bubble coalescence in the upper levels of the flow marked by the depletion of bubbles of intermediate size (decreasing frequency for bubbles equal to or less than the median diameter) and corresponding enrichment in the largest bubble sizes (Mangan, Cashman & Newman, 1993).

The fact that the distribution of the vesicles with diameters less than or equal to the median diameter observed at the bottom of the flow is retained in the upper levels suggest that these vesicles were originally formed by degassing and growth and later subjected to the coalescence process described above and that they form the initial vesicle population. Therefore, the well-sorted vesicle size distribution at the bottom of the flow (Fig. 5c) will be taken as the reference for bubble nucleation and growth study.

5.c. Bubble nucleation

The vesicle size distribution is described by a population density function (Mangan, Cashman & Newman, 1993):

$$n = n_0 \exp\left(-\frac{L}{Gt}\right) \tag{13}$$

where n is the number of bubbles of a given size per unit of volume, n_0 is the number of nuclei, L is the bubble diameter (cm), G is the growth rate of bubbles (cm/s), and t (s) is the time available for nucleation and growth. The plot of ln n versus L is linear with a slope $-\frac{1}{Gt}$ and intercepts ordinate at n_0. The fitting of the linear part of ln n versus bubble diameter in sample 7 has a slope $-\frac{1}{Gt} = -34.26$, $Gt = 2.9 \times 10^{-2}$ cm, and intercepts ordinate (ln n_0) at 15.09, that is, $n_0 = 3.57 \times 10^6$ nuclei per litre of magma. The total number of bubbles ($Nt = n_0 Gt$) is 1.04×10^5 per litre, in good agreement with that measured on the thin-section (1.18×10^5). The time available for the nucleation and growth of the initial bubbles estimated from equation (13) below and assuming an initial bubble radius of 50 microns (Aubele, Crumpler & Elston, 1988) is 10 seconds; the nucleation and growth rate (G) derived from Gt is 2.90×10^{-3} cm/s with a nucleation rate ($n_0 G$) of 10353 events per litre per second. These data are lower than those recorded from lava flows emerging from surface

https://doi.org/10.1017/S001675680600269X Published online by Cambridge University Press

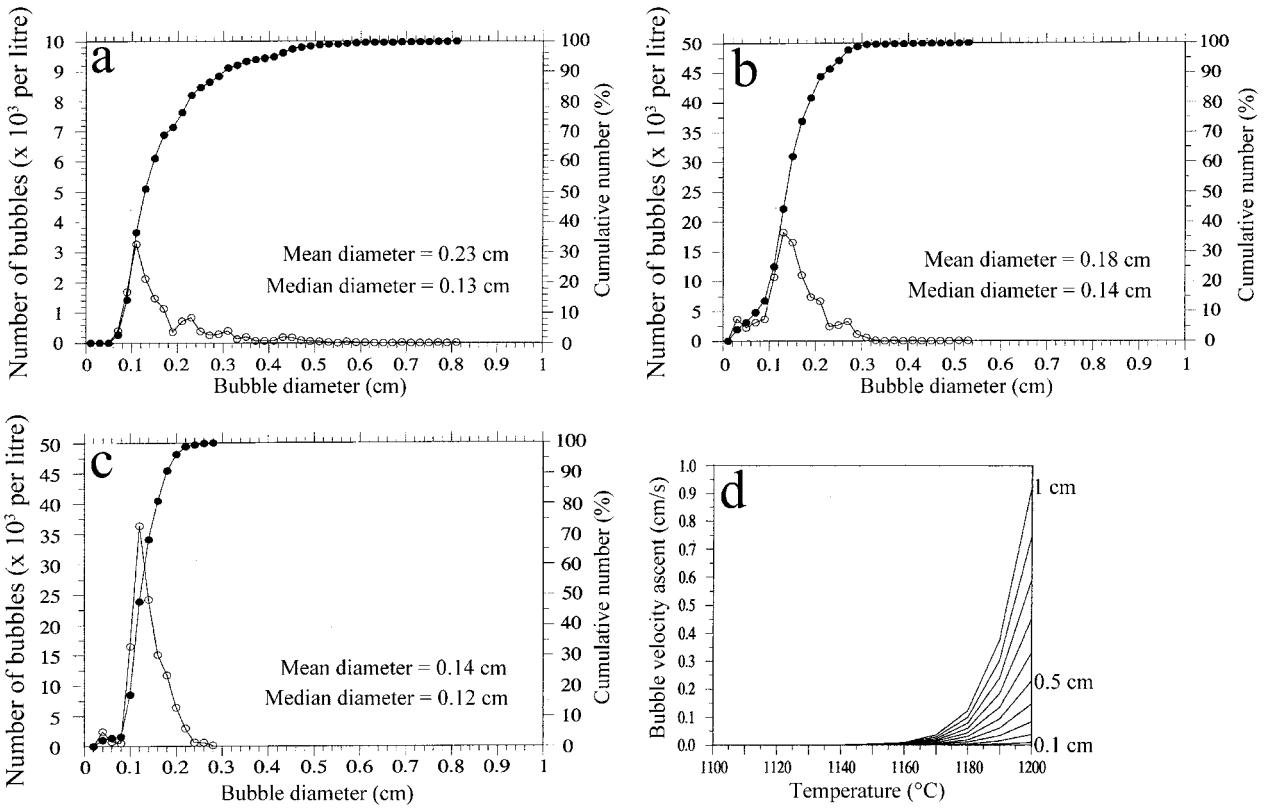

Figure 5. Vesicle size distribution of vesicles and ascent velocities of bubbles: (a–c) size frequency (open circles; left axis) and cumulative number (solid circles; right axis) of vesicles in (a) sample 1, (b) sample 3 and (c) sample 7; (d) ascent velocity of bubbles as a function of magma temperature and bubble radius.

breakout in lava tubes and sampled close to the point of effusion (Cashman, Mangan & Newman, 1994), but the same authors noticed that vesicle number densities may have values less than 10^5 per litre in subaerial lava flows with decreasing nucleation rates to minimum rates of 8000 to 7000 events per litre per second, results in good agreement with those obtained from sample 7.

5.d. Growth time duration

The growth of bubbles is the result of the diffusion of gas dissolved in the magma (diffusive growth) and its decompression within the bubble when hydrostatic pressure decreases (decompressive growth). Two stages of bubble growth can be distinguished during volcanism events as a function of magma decompression. The first stage is a very fast decompression with the ascent of the saturated magma in the volcanic conduit and its eruption. This magma, initially saturated at high pressure, becomes oversaturated due to a large pressure decrease (from 100 to 0.1 MPa) with the maximum of nucleation and growth rate of bubbles (CO_2 and H_2O). This first decompressive growth is usually modelled using a logarithmic law (Proussevitch & Sahagian, 1998; Liu & Zhang, 2000). The second stage operates after eruption during the cooling of the flow. In these conditions, the pressure ranges from about 1 to 0.1 MPa and the derivative of the logarithmic growth law is linear. The geode formation takes place at the time of lava flow emplacement and belongs to the second degassing stage within low pressure values and slow decompression. In these conditions, the degassing process is mainly controlled by thermal diffusion. The change of bubble radius by diffusive growth is given by

$$R_t = R_{t-\Delta t} + (D^{0.5}\,\Delta t)/t^{0.5} \qquad (14)$$

where R_t (cm) is the bubble radius at time t, t (s) is the growth time duration, Δt (s) is the time increment and D is the diffusion coefficient (cm^2/s). Bubble radius at time $t = 0$ was taken to be 50 μm. The diffusion coefficient is calculated from the equation of Sparks (1978):

$$-\log_{10} D = \log_{10}\mu + 5.82 - \frac{4100}{T} \qquad (15)$$

where μ is the viscosity in poise and T the temperature in K. The viscosity is calculated from the equation derived by Aubele, Crumpler & Elston (1988) for magma at temperature less than liquidus temperature:

$$\mu = \mu_0 \exp\left(\frac{26500}{T}\right) + \exp(195 - 0.130T) \qquad (16)$$

where μ_0 is the viscosity at infinite temperature and T the temperature in K. The change of bubble radius by

https://doi.org/10.1017/S001675680600269X Published online by Cambridge University Press

decompressive growth is given by

$$R = R_0 \left(\frac{P_0}{P} \right)^{\frac{1}{3}} \quad (17)$$

where R_0 is the initial bubble radius (cm), and P_0 and P are the initial pressure and the pressure at the considered level in the flow, respectively.

As discussed above, vesicles from sample 7 are taken as the reference for bubble nucleation and growth. Their maximum radius is 0.135 cm. The ascent speed calculated for these bubbles ranges from 0.016 at 1200 °C to 4.90×10^{-5} cm/s at 1150 °C. These bubbles can then be considered to be immobile in the flow and expand only by the diffusive growth process. The time needed for these bubbles to grow from 50 μm (nucleus radius) to 0.135 cm in radius was calculated from equation 14. The result is 7384 seconds at 1200 °C which is the maximum time duration for dominating diffusive growth of bubbles within the flow. Beyond this critical radius, bubbles will continue to grow only by depressurization, allowing their ascent in the flow and the beginning of the coalescence process.

5.e. Bubble ascent in the flow

The velocity of bubble ascent in the magma will depend mainly on the magma and gas properties (viscosity, density), and radius of the bubble, but also on the surface tension at the gas–magma interface. Several equations were experimentally derived for these variables and summarized by Sparks (1978). Aubele, Crumpler & Elston (1988) reduced these equations to:

$$V = 589 \left(\frac{R^2}{\mu} \right) \quad (18)$$

where V is the ascent velocity (cm/s) of the bubble of radius R (cm) in a magma with viscosity μ (poise). The ascent velocities of bubbles with radii ranging from 0.10 to 1.00 cm are plotted versus temperature (°C) in Figure 5d. It appears that 1150 °C is the limit of temperature for bubble ascent, whatever the bubble radius. As a consequence, the 1150 °C isothermal line will be considered as a 'bubble-freezing line' in the modelling of bubble ascent illustrated in Figure 6.

6. Discussion and conclusions

6.a. Origin of the vesicles

The positions of bubbles in the lava flow as a function of cooling time were first calculated for nucleation at times $t = 0$, $t = 6000$, $t = 7000$ seconds, respectively (Fig. 6a, b, c), and at time $t = 7342$ seconds, that is, nucleation of the 0.01 cm radius bubble 42 seconds before the end of gas diffusion (Fig. 6d). Such different nucleation time origins allow simulation of the formation of the vesicular levels observed at the outcrop. Most of the upper coarsely vesicular level was formed by bubbles nucleated at time $t = 0$ from the entire lava flow levels (Fig. 6a). The last migrating bubble was 'frozen' at 1.80 m depth (sample 1) when the temperature reached 1150 °C. It was nucleated at 30 m depth. This bubble had expanded at that time to a maximum radius of 0.19 cm. The upper finely vesicular level was formed predominantly by bubbles which nucleated later ($t = 6000$ seconds, Fig. 6b) from 29 to 15 m depths. The last migrating bubble was 'frozen' at 5 m depth (sample 3) and was nucleated at 29 m depth. This bubble has reached a maximum radius of 0.052 cm. The level with the geodic cavities began to form at time $t = 7000$ seconds with bubbles originating from 29 to 25 m depths and respectively trapped at 7 and 8 m depth (Fig. 6c). The lower finely vesicular level was mainly generated by the last nucleated bubbles, just before the end of gas diffusion at time $t = 7384$ seconds. Growth decompression was nearly the only process undergone by these bubbles, inducing very low growth rates, and hence, very short ascent. The simulation of this lower finely vesicular level was achieved using bubbles with the smallest radius measured on sample 7 (0.01 cm), nucleated 42 seconds before the end of gas diffusion. The simulation illustrated in Figure 6d indicates that the lower finely vesicular level is formed by bubbles nucleated at 30 to 28 m depths and trapped between 30 to 27 m with a maximum radius of 0.015 cm.

At the end of bubble ascent, this model simulates a vesicle-free central part between 12 and 27 m depths which is observed at the outcrop (Fig. 1b). However, the maximum bubble radii calculated for each level using diffusive/decompressive bubble growth are always smaller than the maximum radii obtained by the image analysis on the same levels. This implies that bubble nucleation and growth are not the only active processes but need to be completed by bubble coalescence, as previously noticed in the study of the vesicle size distribution. The bubble coalescence was much more active in the upper vesicular levels than in the lower one, as outlined by the increasing discrepancies between calculated and measured maximum radii (Table 2) from the bottom to the top of flow: 0.015 cm versus 0.14 cm, 0.052 cm versus 0.26 cm and 0.19 cm versus 0.40 cm for samples 7, 3 and 1, respectively.

The level with the geodic cavities is more distinctive, with 0.043 cm maximum bubble radius as calculated using the diffusive/decompressive bubble growth versus 17.68 cm as measured mean radius for the geodic cavities (Table 3). Such a large discrepancy in the radii cannot be explained by bubble coalescence alone and requires an additional bubble accumulation process below the 1150 °C barrier, as discussed below. An important result derived from Figure 6 is the initial nucleation depth interval for bubbles forming the different vesicular and geodic levels. The total amount of water vapour available for the considered vesicular level can be estimated by the integration of the water

https://doi.org/10.1017/S001675680600269X Published online by Cambridge University Press

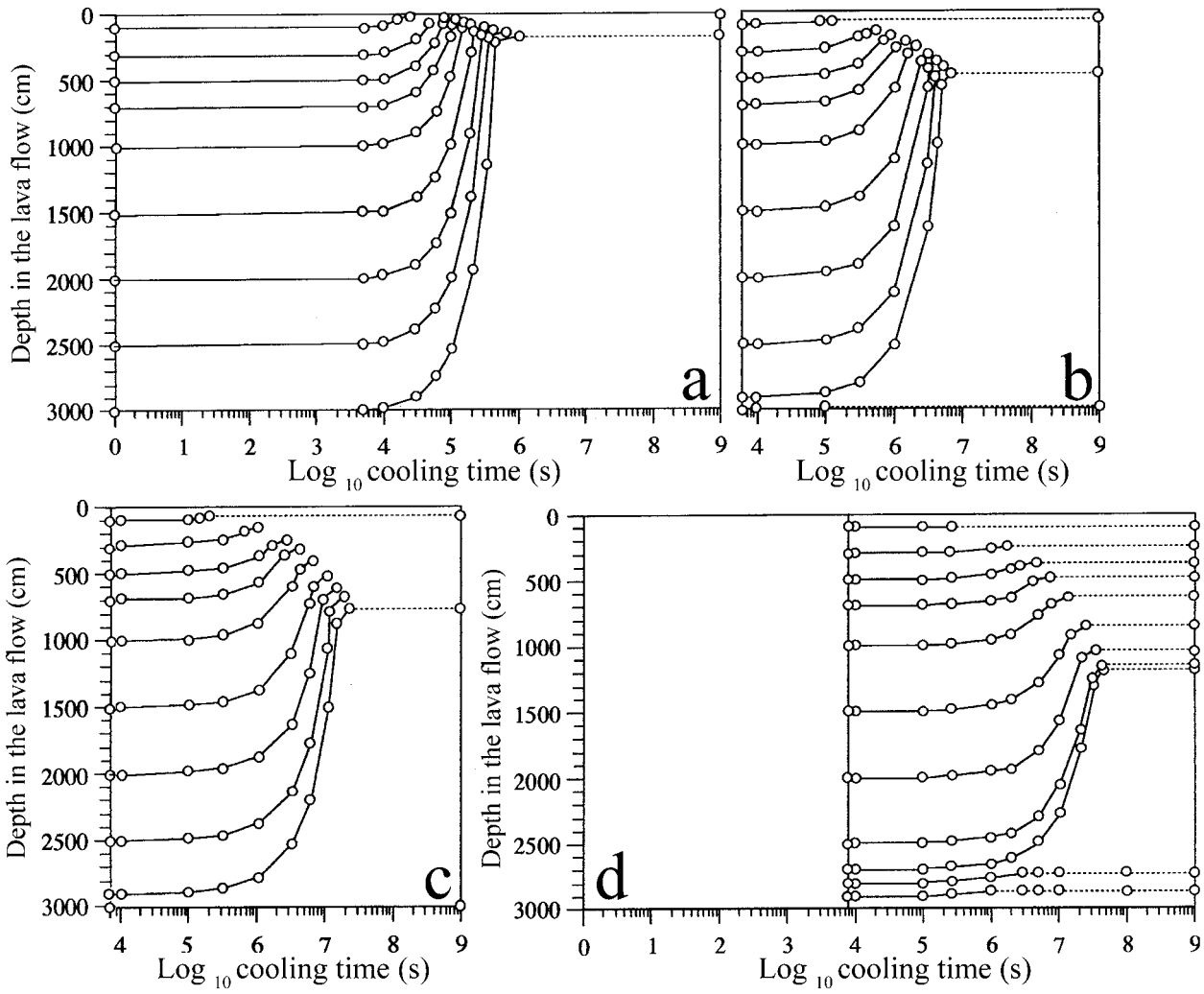

Figure 6. Simulation of bubble ascent in the lava flow as a function of cooling time: (a) bubbles nucleated at time $t = 0$; (b) bubbles nucleated at time $t = 6000$ s; (c) bubbles nucleated at time $t = 7000$ s; (d) position of the 0.01 cm radius bubble in the lava flow as a function of cooling time.

Table 2. Image analysis data of thin sections from vesicular levels

Samples (see Fig. 2)	Depth in the flow (cm)	Vesicularity (%)	Number of vesicles (per litre of melt)	Volume of vesicles (cm^3 per litre of melt)	Mean radius (cm)*	Maximum radius (cm)
1	180	11	1.46×10^4	103.71	0.12 (0.07)	0.40
3	500	28	1.48×10^5	261.48	0.09 (0.03)	0.26
7	2720	18	1.18×10^5	164.55	0.07 (0.02)	0.14

*values in parentheses are standard deviations.

Table 3. Image analysis data of photographs from mining galleries

Galleries* (see Fig. 2)	Mean radius (cm)	Maximum radius (cm)	Mean distance between geodes (cm)	Mean volume (cm^3)
Geodes (1)	10.45	16.15	60.61	8.11×10^4
Geodes (2)	9.30	14.45	73.98	4.37×10^3
Geodes (3)	16.80	31.93	111.88	4.00×10^4
Geodes (4)	22.21	32.99	108.27	6.22×10^4
Geodes (5)	17.18	27.49	76.86	2.90×10^4
All geodes	17.68	32.99	78.85	2.31×10^4

*Numbers in parentheses refer to mining galleries in Figure 2a.

https://doi.org/10.1017/S001675680600269X Published online by Cambridge University Press

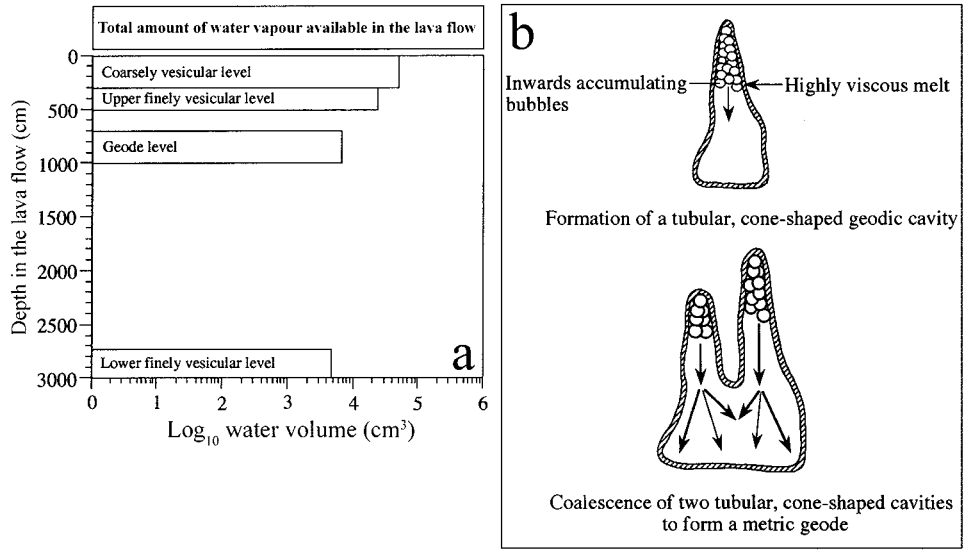

Figure 7. Volume of water vapour needed for the vesicular levels formation and cone-shaped geode formation: (a) volume of water vapour calculated by integrating the volume of vesicles obtained from sample 7 image analysis (see Table 2) along a melt column with 10 cm square section and nucleation depth as height (Table 4); (b) inwards growth of the cone-shaped cavities and their coalescence into large metre-sized geodes.

Table 4. Amounts of water vapor (cm^3) exsolved from the lava flow

Lava flow levels (see Fig. 1b)	Depth (cm)	Thickness (cm)	Nucleation depth (cm)	Volume of exsolved water vapour (cm^3)*	Volume of exsolved water vapour (cm^3)**	Total volume of exsolved water vapour (cm^3)
Upper coarsely vesicular level	0–300	300	0–3000	4.94×10^4	1.17×10^6	1.17×10^6
Upper finely vesicular level	300–500	200	1500–2900	2.30×10^4	1.08×10^5	
Geodes level	700–1000	300	2500–2900	6.58×10^3	8.45×10^3	
Lower vesicular level	2700–3000	300	2800–3000	4.61×10^3	4.01×10^3	

*Calculation using the volume of vesicles in sample 7 as reference.
**Calculation using the volume of H_2O vapour exsolved per litre of magma.
All calculations were achieved using a melt column reference of 100 cm^2 basal section and the nucleation depth interval as height.

vapour exsolved as a function of depth in the flow (Fig. 7a) along a melt column with a 10 cm square section and height as the nucleation depth interval. The calculation achieved for the lower finely vesicular level gives 4.01×10^3 cm^3 of water vapour available for bubble formation in this level, whereas integration on the same melt column (30 m to 27.20 m depths) using vesicle volume measured from image analysis of sample 7 (164.55 cm^3 per litre of melt, Table 2) gives 4.6×10^3 cm^3 of water vapour. These results are in the same order of magnitude and indicate that the amount of water vapour available at the time of lava emplacement between the 30 m and 27.20 m depths has been retained in the lower finely vesicular level. The vesicle volumes measured for samples 3 and 1 are close to those from sample 7 (261.48 and 103.71 cm^3 per litre of melt, respectively, in Table 2). Thus, vesicle volume measured for sample 7 will be taken as reference for calculations in the upper levels.

The calculations using water vapour exsolved as a function of depth, and measured vesicle volumes, are compared in Table 4 and illustrated in Figure 7a. The volume of water vapour needed for the formation of the different vesicular levels is always equal to or lower than the volume of water vapour available in the lava at time of its emplacement. The total volume of water vapour available in the entire melt column with 100 cm^2 section and 3000 cm height reaches 1.17×10^6 cm^3, whereas the total volume of water vapour trapped in vesicles and geodes reaches 83.59×10^4 cm^3, 7 % of the total water vapour available. As a conclusion on the origin of the vesicles, it can be noted that (1) the vesiculation of a lava flow is a short-lived process when compared to the solidification time of the lava; the vesicle distribution actually observed in the solidified lava is completed after about 10^7 seconds (or 4 months) cooling time versus about 38×10^7 seconds (or 12 years) for the lava to solidify; (2) the amount of water vapour exsolved by the magma is sufficient to explain the formation of the oberved vesicles, as well as the geodic cavities, with no need for external supply of surface water; (3) the order of vesicular level formation obtained with the model is: upper coarsely vesicular level, finely vesicular levels and finally, levels with geodic cavities. This model simulates a vesicle-free central part between the 12 and 27 m depths, as

https://doi.org/10.1017/S001675680600269X Published online by Cambridge University Press

observed at the outcrop. Moreover, this vesiculation order fits with the calculated decreasing solidification rates, from 0.11 cm/h at the top of the flow to 0.01 cm/h in the central part.

6.b. Origin of the geodic cavities

Currently, the most widely proposed origin for the abnormally large vesicle cylinders in basaltic lava flows is the interaction of the flowing lava with surface water or a water-rich substratum during emplacement. This water–lava interaction results in the injection of non-magmatic gas into the flow through cracks in the base before completion of interior flow consolidation. Subsequent rise and solidification isolate the resulting vesicle column from the associated base crack (Walker, 1987; McMillan, Long & Cross, 1989). Detailed studies of vesicle cylinders (MacDonald, 1968; Petrov, 1984) indicate, however, that these large rising gas bubbles originating in the lower part of the flow leave behind them a track of small vesicles, the porous cylinder, and spiracles, which are open parts of the cavities extending to the base of the lava flow. Neither pillow lavas nor quenched basaltic layers have been observed in the lower vesicular levels from the visited flows, which could account for the interaction of the lava with surface water at the bottom of the flow. Duarte, Hartmann & Vasconcellos (2005) proposed an epigenetic origin for the geodic cavities based upon several types of evidence: (1) low temperature mineralogy in the geodes ($< 100\,^{\circ}$C), ruling out the opening of the cavities at magmatic temperatures; (2) occurrence of subhorizontal hydraulic fractures below the geodes which can act as feeding channels of the geodes and could be indicative of cooling to brittle conditions; (3) widespread occurrence of hydraulic breccias at the bottom of the flows indicative of explosive activity in relation to geode formation and (4) a mineralizing fluid originating in the Guarany aquifer. Our recent fluid inclusion studies in amethyst crystals and geochemical mass balances in the geode-bearing basaltic massive level (to be published) indicate that (1) amethyst crystallization temperatures are in the range 204–238 °C, (2) the silicon released by the basalt alteration in the vicinity of the geodes is sufficient to explain their siliceous crystallization and (3) the process of geode formation operates at magmatic temperatures, whereas siliceous crystallizations occur at temperatures between 204 and 238 °C. Moreover, no hydraulic breccia was observed at the base of the geode which could account for a feeding channel and indicate cooling to brittle conditions before geode formation. Basaltic breccias are frequently observed at the bottom of the flows but they are breccias formed during the flow of lava; they incorporate rounded sandstone blocks and not angular fragments which are characteristics of hydraulic breccias related to explosive activity. Finally, the positions of the four flows with amethyst economic importance are flows 4, 6, 8 and 9 in the basaltic pile composed of 12 conformable horizontal flows (Gomes *et al.* 2005). The occurrence of a mineralizing fluid that originated in the Guarany aquifer appears unlikely since (1) fluids would have to pass through three flows (about 140 m global thickness) before forming geodes and crystallizing amethyst in the first geode-bearing flow and (2) the results herein support the idea that water vapour needed for geode formation is exsolved from the lava flow itself.

In these conditions, the only other possibility for water vapour feeding of the geodic cavities must be sought in the magmatic gas exsolving from the supersaturated melt with respect to dissolved volatiles (Sparks, 1978). The main question is whether a sufficient amount of water vapour can be exsolved from the lava flow to produce such abnormally large geodic cavities. The discussion of this problem is based upon (1) the distribution pattern of the geodic cavities, as observed in five mining galleries (Fig. 2a) and studied using image analysis procedures (Table 3), and (2) the quantity of magmatic water vapour available at the depth of the geodes level, as given in Table 4 and Figure 7a.

The mean radius of the equivalent sphere derived from image analysis data of the geodic cavities (Table 3) is 17.68 cm. The mean distance (with no visible vesiculation) between the geodes is 78 cm, indicating that the mean geode will form by trapping bubbles in a column with 39 cm radius basal section. The quantity of water vapour available at the geodes level is 6.58×10^3 cm^3 (Table 4), calculated for a reference melt column with 100 cm^2 section and 400 cm height (geodes are forming from bubbles originating from 29 m to 25 m depths). The quantity of water vapour exsolved by a cylindrical melt column with the same height and a basal radius of 39 cm is 3.14×10^5 cm^3 and is sufficient to produce about thirteen geodes with 17.68 cm radius. This quantity of vapour is also sufficient to produce two geodes with the largest observed radius, 33 cm. The special vertically oriented habit of the geodic cavities with downwards-increasing diameters and branching parts can be explained by the pipe vesicle formation model of Philpotts & Lewis (1987). In this model, magma in contact with the first bubble trapped will cool more rapidly by radiating heat to the cooler side (upper side) of the bubble than the surrounding magma out of contact. A more viscous zone is then produced at the top of the trapping level, allowing bubbles to accumulate below this level. The same process is repeated as bubbles accumulate with subsequent increase in the width of the more viscous zone inwards in the flow, until the end of gas exsolution.

The net result of such processes is the formation of geodic cavities with cone-shaped habits. This particular habit can also partly result from bubble coalescence which can occur before final bubble emplacement and give geodes their hydrodynamic shapes. The bases of these geodes display a particular upward convex

https://doi.org/10.1017/S001675680600269X Published online by Cambridge University Press

shape which was reported by Duarte, Hartmann & Vasconcellos (2005) to coincide with a hydraulic fracture which could act as a feeding channel for fluids and later ore deposition in the geodes. Study of the geode distribution in the five mining galleries of the Triz quarry did not show evidence of hydraulic fracturing at the bottom of the geodes but rather of a regular and undisturbed thin green celadonite layer rim enclosing the geode in the massive basalt. This clayey rim is strictly associated with the geode and appears as the initial, non-fractured basaltic wall of the geode previously altered into celadonite by the hydrothermal fluids trapped in the geode. In this non-fractured context, the peculiar upward-convex bottom of the geodes could be explained by the higher cooling rate of the basaltic magma at the centre of the geode base in contact with large vapour volume than the magma at the periphery where the contact with volume vapour is more limited and radiating heat loss is smaller.

The occurrence of metre-sized geodic cavities with branching parts is well explained by the junction of several inwards-progressing tubular cavities at the bottom of the trapping level (Fig. 7b).

As a conclusion on the origin of the geodic cavities, it can be emphasized that (1) the formation of geodes in this lava flow can be entirely explained, qualitatively and quantitatively, by the exsolution of magmatic gas from the supersaturated melt with no need for external surface water supply; (2) the particular tubular habit of the geodes results from the higher cooling rate of the magma in contact with the accumulating bubbles; and (3) the abnormal metre-sized geodes do not result from the diffusive/decompressive bubble growth but from the coalescence of inwards-progressing tubular cavities.

References

ANDERSON, A. T. 1975. Some basaltic and andesitic gases. *Reviews of Geophysics and Space Physics* **13**, 37–55.

ANDERSON, A. T., SWIHART, G. H., ARTIOLI, G. & GEIGER, C. A. 1984. Segregation vesicles, gas-filter-pressing, and igneous differentiation. *Journal of Geology* **92**, 55–72.

AUBELE, J. C., CRUMPLER, L. S. & ELSTON, W. E. 1988. Vesicle zonation and vertical structure of basalt flows. *Journal of Volcanology and Geothermal Research* **35**, 349–74.

BELLIENI, G., COMIN-CHIARAMONTI, P., ERNESTO, M., MELFI, A. J., PACCA, I. G. & PICCIRILLO, E. M. 1984. Flood basalt to rhyolite suites in the southern Paraná plateau (Brazil): paleomagnetism, petrogenesis and geodynamic implications. *Journal of Petrology* **25**, 579–618.

BERESFORD, S. W., CAS, R. A. F., LAMBERT, D. D. & STONE, W. E. 2000. Vesicles in thick komatiite lava flows, Kambalda, Western Australia. *Journal of the Geological Society, London* **157**, 11–14.

BOTTINGA, Y. & JAVOY, M. 1990. Mid-Ocean Ridge basalt degassing: Bubble nucleation. *Journal of Geophysical Research* **95**, 5125–31.

BURNHAM, C. W. 1979. The importance of volatile constituents. In *The Evolution of the Igneous Rocks – Fiftieth Anniversary Perspectives* (ed. H. S. Yoder Jr), pp. 439–82. Princeton University Press.

BURNHAM, C. W. & JAHNS, R. H. 1962. A method for determining the solubility of water in silicate melts. *American Journal of Science* **260**, 721–45.

CASHMAN, K. V. & KAUAHIKAUA, J. P. 1997. Reevaluation of vesicle distributions in basaltic lava flows. *Geology* **25**, 419–22.

CASHMAN, K. V., MANGAN, M. T. & NEWMAN, S. 1994. Surface degassing and modification to vesicle size distributions in active basalt flows. *Journal of Volcanology and Geothermal Research* **61**, 45–68.

CASHMAN, K. V. & MARSH, B. 1988. Crystal size distribution (CSD) in rocks and the kinetics and dynamics of crystallization: II. Makaopuhi lava lake. *Contributions to Mineralogy and Petrology* **99**, 292–305.

DEGRAFF, J. M., LONG, P. E. & AYDIN, A. 1989. Use of joint-growth directions and rock textures to infer thermal regimes during solidification of basaltic lava flows. *Journal of Volcanology and Geothermal Research* **38**, 309–24.

DUARTE, L. D. C., HARTMANN, L. A. & VASCONCELLOS, M. A. Z. 2005. Epigenetic geode formation in the world-class amethyst deposits of the southern Paraná basaltic province. In *I Simpósio Brasileiro de Metalogenia, 2005, Gramado*. CD-ROM. Porto Alegre. *Sociedade Brasileira de Geologia.*

ERNESTO, M. & PACCA, I. G. 1988. Paleomagnetism of the Paraná basin flood volcanics, southern Brazil. In *The Mesozoic flood volcanism of the Paraná basin: petrogenetic and geophysical aspects* (eds E. M. Piccirillo and A. J. Melfi), pp. 229–55. Universidade de Sao Paulo, Brazil.

GERLACH, T. 1986. Exsolution of H_2O, CO_2, and S during eruptive episodes of Kilauea volcano, Hawaii. *Journal of Geophysical Research* **91**, 12177–85.

GILG, H. A., MORTEANI, G., KOSTITSYN, Y., PREINFALK, C., GATTER, I. & STRIEDER, A. J. 2003. Genesis of amethyst geodes in basaltic rocks of the Serra Geral Formation (Ametista do Sul, Riuo Grande do Sul, Brazil): a fluid inclusion, REE, oxygen, carbon, and Sr isotope study on basalt, quartz, and calcite. *Mineralium Deposita* **38**, 1009–25.

GOFF, F. 1996. Vesicle cylinders in vapour-differentiated basalt flows. *Journal of Volcanology and Geothermal Research* **71**, 167–85.

GOMES, M. E. B., MEXIAS, A. S., SCOPEL, R., BONGIOLO, E. M., FORMOSO, M. L. L. & MILARA, T. 2005. Volcanic sequence of the amethyst district in South Paraná Province, Rio Grande do Sul, Brazil: Flow emplacement mechanisms and geodes formation. In *I Simpósio Brasileiro de Metalogenia, 2005, Gramado*. CD-ROM. Porto Alegre. Sociedade Brasileira de Geologia.

GROSSENBACHER, K. A. & MCDUFFIE, S. M. 1995. Conductive cooling of lava: columnar joint diameter and stria width as functions of cooling rate and thermal gradient. *Journal of Volcanology and Geothermal Research* **69**, 95–103.

HAMILTON, D. L., BURNHAM, C. W. & OSBORN, E. F. 1964. The solubility of water and effects of oxygen fugacity and water content on crystallization in mafic magmas. *Journal of Petrology* **5**, 21–39.

HARDEE, H. C. & DUNN, J. C. 1981. Convective heat transfer in magmas near the liquidus. *Journal of Volcanology and Geothermal Research* **10**, 195–207.

HARRIS, D. M. & ANDERSON, A. T. 1983. Concentrations, sources, and losses of H_2O, CO_2, and S in Kilauean basalt. *Geochimica Cosmochimica Acta* **47**, 1139–50.

JAEGER, J. C. 1961. The cooling of irregularly shaped igneous bodies. *American Journal of Science* **259**, 721–34.

JAEGER, J. C. 1968. Cooling and solidification of igneous rocks. In *Basalts: The Poldervaart Treatise on Rocks of Basaltic Composition. Volume 2* (eds H. H. Hess and A. Poldervaart), pp. 503–36. New York, NY: John Wiley & Sons, Inc.

LIU, Y. & ZHANG, Y. 2000. Bubble growth in rhyolitic melt. *Earth and Planetary Science Letters* **181**, 251–64.

LONG, P. E. & WOOD, B. J. 1986. Structures, textures, and cooling histories of Columbia River basalt flows. *Geological Society of America Bulletin* **97**, 1144–55.

LORE, J., HUAJIAN-GAO, H. J. & AYDIN, A. 2000. Viscoelastic thermal stress in cooling basalt flows. *Journal of Geophysical Research Solid Earth* **105**, 23695–709.

MACDONALD, G. A. 1968. Forms and structures of extrusive basaltic rocks. In *Basalts: The Poldervaart Treatise on Rocks of Basaltic Composition. Volume 2* (eds H. H. Hess and A. Poldervaart), pp. 1–60. New York, NY: John Wiley & Sons, Inc.

MANGAN, M. T., CASHMAN, K. V. & NEWMAN, S. 1993. Vesiculation of basaltic magma during eruption. *Geology* **21**, 157–60.

MCMILLAN, K., CROSS, R. W. & LONG, P. E. 1987. Two-stage vesiculation in the Cohassett flow of the Grande Ronde Basalt, south-central Washington. *Geology* **15**, 809–12.

MCMILLAN, K., LONG, P. E. & CROSS, R. W. 1989. Vesiculation in Columbia River basalts. In *Volcanism and tectonism in the Columbia River flood-basalt province* (eds S. P. Reidel and P. R. Hooper), pp. 157–67. Geological Society of America, Special Paper no. 239.

MELFI, A. J., PICCIRILLO, E. M. & NARDY, A. J. R. 1988. Geological and magmatic aspects of the Paraná basin. An introduction. In *The Mesozoic flood volcanism of the Paraná basin: petrogenetic and geophysical aspects* (eds E. M. Piccirillo and A. J. Melfi), pp. 1–13. Universidade de Sao Paulo, Brazil.

MOORE, J. G. 1970. Water content of basalt erupted on the ocean floor. *Contributions to Mineralogy and Petrology* **28**, 272–9.

MURASE, T. & MCBIRNEY, A. R. 1973. Properties of some common igneous rocks and their melts at high temperatures. *Geological Society of America Bulletin* **84**, 3563–92.

PATRICK, M. R., DEHN, J. & DEAN, K. 2004. Numerical model of lava flow cooling applied to the 1997 Okmok eruption: Approach and analysis. *Journal of Geophysical Research* **109**, B03202.1–17.

PECK, D. L. 1978. *Cooling and vesiculation of Alae Lava Lake, Hawaii*. United States Geological Survey Professional Paper, 935-B, 59 pp.

PECK, D. L., HAMILTON, M. S. & SHAW, H. R. 1977. Numerical analysis of lava lake cooling models: part II, application to Alae lava lake, Hawaii. *American Journal of Science* **277**, 415–37.

PETROV, V. P. 1984. Tubular cavities and porous cylinders in lavas and their petrogenetic significance. *Izvestiya AN SSSR, seriya geologiya* **4**, 42–9 (Russian translation).

PHILPOTTS, A. R. & DICKSON, L. D. 2002. Millimetre-scale modal layering and the nature of the upper solidification zone in thick flood-basalt flows and other sheets of magma. *Journal of Structural Geology* **24**, 1171–7.

PHILPOTTS, A. R. & LEWIS, C. L. 1987. Pipe vesicles – an alternate model for their origin. *Geology* **15**, 971–4.

PROUSSEVITCH, A. A. & SAHAGIAN, D. L. 1998. Dynamics and energetics of bubble growth in magmas: analytical formulation and numerical modeling. *Journal of Geophysical Research* **103**, 18223–51.

REITER, M., BARROLL, M. W., MINIER, J. & CLARKSON, G. 1987. Thermo-mechanical model for incremental fracturing in cooling lava flows. *Tectonophysics* **142**, 241–60.

SAHAGIAN, D. L. 1985. Bubble migration and coalescence during the solidification of basaltic lava flows. *Journal of Geology* **93**, 205–11.

SAHAGIAN, D. L., ANDERSON, A. T. & WARD, B. 1989. Bubble coalescence in basalt flows: comparison of a numerical model with natural examples. *Bulletin of Volcanology* **52**, 49–56.

SCOPEL, R. M., GOMES, M. E. B. G., FORMOSO, M. L. L. & PROUST, D. 1998. Derrames portadores de ametistas na região de Frederico Westphalen-Irai-Planalto-Ametista do Sul, RS-Brasil. *Congreso Uruguaio de Geologia 2, Actas*, 243–52.

SIGVALDASON, G. E. & ELISSON, G. 1968. Collection and analysis of volcanic gases at Surtsey, Iceland. *Geochimica et Cosmochimica Acta* **32**, 797–805.

SPARKS, R. S. J. 1978. The dynamics of bubble formation and growth in magmas: a review and analysis. *Journal of Volcanology and Geothermal Research* **3**, 1–37.

STOLPER, E. & HOLLOWAY, J. R. 1988. Experimental determination of the solubility of carbon dioxide in molten basalt at low pressure. *Earth and Planetary Science Letters* **87**, 397–408.

TORAMARU, A. 1989. Vesiculation process and bubble size distributions in ascending magmas with constant velocities. *Journal of Geophysical Research* **94**, 17523–42.

TURNER, S., REGELOUS, M., KELLEY, S., HAWKESWORTH, C. & MANTOVANI, M. 1994. Magmatism and continental break-up in South Atlantic high precision $^{40}Ar/^{39}Ar$ geochronology. *Earth and Planetary Science Letters* **121**, 333–48.

WALKER, G. P. L. 1987. Pipe vesicles in Hawaiian basaltic lavas: their origin and potential as paleoslope indicators. *Geology* **15**, 84–7.

WALKER, G. P. L. 1989. Spongy pahoehoe in Hawaii: a study of vesicle-distribution patterns in basalt and their significance. *Bulletin of Volcanology* **51**, 199–209.